DOE/PC/79903--T16

DOE/PC/79903--T16

DE92 041305

OPTICAL PROPERTIES OF FLYASH

Contract No. DE-AC22-87PC 79903

Quarterly Report for Period 1 October – 31 December 1989

Prepared for Pittsburgh Energy Technology Center

Principal Investigator Professor S. A. Self

January 1990

HIGH TEMPERATURE GASDYNAMICS LABORATORY
Mechanical Engineering Department
Stanford University

OPTICAL PROPERTIES OF FLYASH
Contract No. DE-AC22-87PC 79903
Quarterly Report for Period 1 October – 31 December 1989
Prepared for Pittsburgh Energy Technology Center
Principal Investigator Professor S. A. Self

EXECUTIVE SUMMARY

The general aims of this research are to provide a fundamental scientific basis for the physical understanding and reliable calculation of radiative heat transfer in coal combustion systems, particularly as it is influenced by the presence of inorganic constituents deriving from the mineral matter in coal.

The work is organized under four tasks. Tasks I and II were initiated in October 1987; Tasks III and IV were funded from October 1988.

Task 1. Characterization of Flyash: Under this heading the chemical composition and size distribution of representative flyashes are being measured by appropriate microanalytical techniques to provide information required in Task 2.

Task 2. Measurements of the Optical Constants of Slags: Under this heading measurements of the infrared optical constants (i.e., the complex refractive index $m = n - ik$) of synthetic slags are being made as a function of wavelength and temperature for controlled compositions. Particular attention will be given to the contribution of the Fe_2O_3 content and its valence state. The data is being reduced to yield formulae giving the complex refractive index over relevant ranges of wavelength and temperature, as a function of the relevant metal oxide constituents.

Task 3. Sample Calculations of the Radiant Properties of Flyash Dispersions: This component comprises various calculations to guide and evaluate the experimental work under the other three tasks.

Task 4. Measurement of the Radiant Properties of Flyash Dispersions: This bench-scale experiment is planned to compare the measured radiant properties of a dispersion of well-characterized ash with computations based on data developed under the first two tasks.

In this ninth quarter good progress has been made in all four areas, as reported in the Quarterly Report, and summarized below.

Task 1

The ashes being characterized are samples from power plants or pilot-scale combustors derived from combustion of six of the coals selected for study under the parallel PETC program on "Transformation of Inorganic Coal Constituents in Combustion Systems."

The principal features requiring characterization are particle size and composition distributions, including correlations between size and composition. Size distributions are being measured in house by Coulter counter. Size and composition distributions are being determined by automated SEM/microprobe analysis at UNDERC. Other in-house characterization work under way includes size classification by wet sieving combined with classification by density using flotation/sedimentation techniques, low temperature ashing for the char content and magnetic separation for the magnetite content resulting from combustion of pyrite.

Size distributions for all six ashes over the range 0.5 – 60 μm have been completed using the Coulter multisizer with a technique employing two orifices to cover the whole range. A suitable technique for matching distributions using two orifice sizes was devised. The measured distribution was found to be very well represented by truncated log-normal distributions. Comparison with the size distribution from automated SEM shows some discrepancy which is still being investigated.

Micrographs of the ash samples prepared by UNDERC for automated SEM/EDX size-composition analysis revealed many agglomerates, casting some doubt on the validity of the data. A freeze-drying technique for sample preparation has been developed at Stanford which gives very well dispersed samples. The automated SEM/EDX analysis has been repeated using such samples and the results have been analyzed using statistical computer codes developed at Stanford. Ternary diagrams of the composition distributions (in color) have been prepared using software developed at Stanford. In the past quarter, automated SEM/EDX analyses have been completed and preliminary analysis of the data made for all six ashes.

In addition, this quarter, density classification results have been obtained for all six ashes and compared with results from SEM analysis for composition, which, of course, determines the density.

Task 2

Methods for determining the infrared optical properties of solid synthetic and natural slags at low temperatures have been established in prior work at Stanford. In the present work the main effort has been devoted to the development of suitable apparatus and

techniques for performing similar measurements on slags at temperatures to 2000K, when the slag is liquid. Basic experimental strategies have been decided and apparatus has been designed to accomplish this task. Preliminary tests at high temperatures during past quarters have resulted in the first reliable measurements of the infrared absorption of liquid slag.

Two complementary techniques involving infrared optical measurements on liquid samples of synthetic slag maintained in an electric furnace have been developed. The first, for the wavelength range 1 – 5 μm where the absorption index is low ($k \leq 10^{-2}$) employs a submerged platinum mirror to measure the absorption of thin films of slag by a double-pass technique. The second, applicable over the whole wavelength range (1–12 μm), measures the surface reflectance of the liquid slag relative to that of a cold gold mirror in an external reference path.

The first technique has been successfully used to obtain the first reliable measurements of the infrared absorption of liquid slag (at 2000 K).

Efforts have since been concentrated on developing and testing the second technique (for surface reflectivity measurements). It was determined that the quality of the data obtained is limited by the differing absorptions due to CO_2 and H_2O in the hot measurement path and the cold reference path. To eliminate this problem, the whole apparatus has been enclosed in a chamber, purged with dry nitrogen.

With this modification, good measurements of the reflectivity of synthetic slag containing 5% Fe at 1600°C were made over the whole wavelength range 1–12 μm. The data in the range 8–12 μm were reduced, using the Kramers–Kronig technique to give both the real and imaginary parts of the complex refractive index.

In the past quarter, possible sources of uncertainty in these measurements have been critically investigated and resolved. In particular, a problem due to contamination of a mirror by furnace gases has been identified and steps taken to eliminate it by redesign of the optical system. Also, in this quarter, reflectance measurements on liquid slags containing zero, 1% and 5% iron (as Fe_2O_3) have been completed. The results have been reduced, using Kramers-Kronig analysis to yield the real (n) and imaginary (k) parts of the complex refractive index.

Task 3

Programs have been written for Mie scattering calculations which are then convolved with input on the size and optical constants distributions for a particulate dispersion to yield the spectral scattering and absorption coefficients of the aerosol. Additionally, a program

has been written to solve the radiation transfer problem for a homogeneous slab, utilizing the exact solution method of Case's normal modes. Input for the spectral scattering and absorption coefficients from the first program allows the spectral scattering, absorption and emission properties of the slab to be computed. These can then be integrated over wavelength to yield the total radiative heat transfer characteristics of the slab.

These programs have been used to determine the importance of certain features of typical ashes for radiation transfer. These include the sensitivity of the optical/radiative properties of a flyash dispersion to (i) composition-size correlation, especially with regard to the distribution of iron oxides with particle size, and (ii) the presence of bubbles in the glassy ash particles.

This computational capability is also being used to evaluate the experimental conditions in the design of the apparatus for Task 4.

Task 4

Careful consideration has been given to the feasibility of various basic approaches for implementing the goals of this task. After evaluating various experimental techniques, a basic approach has been identified, which involves extinction measurements on flyash dispersed in suitable organic liquids. Measurements of the infrared transmission of three selected liquids have been made which confirm their suitability for this purpose. In the past quarter, CaF2 windows for an absorption cell have been acquired and preliminary tests of a suitable cell design have been made.

1.0 INTRODUCTION

This is the ninth quarterly report under DOE contract No. DE-AC22-87PC 79903 entitled "Optical Properties of Flyash." Tasks 1 and 2 of this program were funded from 15 September 1987. Tasks 3 and 4 were funded from 15 September 1988.

The general aims of this research are to provide a fundamental scientific basis for the physical understanding and reliable calculation of radiative heat transfer in coal combustion systems, particularly as it is influenced by the presence of inorganic constituents deriving from the mineral matter in coal. Some preliminary work in this area has been carried out at Stanford in the past several years with NSF support. The present program will greatly enlarge the scope of this work.

The complete, integrated program of theoretical and experimental work comprises four separate tasks.

Task 1. Characterization of Flyash

Task 2. Measurements of the Optical Constants of Slags

Task 3. Sample Calculations of the Radiant Properties of Flyash Dispersions.

Task 4. Measurements of the Radiative Properties of Flyash Dispersions.

In Task 1, the chemical composition and size distribution of representative flyashes are being measured by appropriate microanalytical techniques to provide information required in Tasks 2 and 3.

In Task 2, measurements of the infrared optical constants (i.e., the complex refractive index $m = n - ik$) of synthetic slags are being made as a function of wavelength and temperature for controlled compositions. Particular attention is being given to the contribution of Fe_2O_3 content and its valence state. The data will be reduced to yield formulae giving the complex refractive index over relevant ranges of wavelength and temperature, as a function of the relevant metal oxide constituents.

In Task 3, sample calculations are being made for typical ash loadings, size distributions and compositions for simple geometries, with two main purposes: first, to provide insight and physical understanding of the role of flyash in radiative heat transfer in combustion systems; second, to indicate the sensitivity of the results to the characteristics of the input data. Such calculations will also be used to determine appropriate conditions and to predict the expected measured radiative properties for the experiment of Task 4.

The experiment of Task 4 is designed to critically test our ability to predict the measured spectral emittance and scattering coefficient of flyash dispersions under well-controlled laboratory conditions utilizing the optical property data developed in Task 2. Particular attention will be paid to assessing the contribution of the char component in typical ashes. Any discrepancies between calculated and measured quantities revealed by these tests will be resolved by appropriate further studies.

A more detailed description of the scope of these tasks is given below. First, however, an outline is given of the rationale for the overall approach adopted in this program.

1.1 Rationale of Overall Approach

To account for the effects of flyash in radiative heat transfer calculations requires a knowledge of the contributions of the ash to the spectral absorption (a_λ) and scattering (σ_λ) coefficients of the particulate dispersion, together with the phase function Φ_λ describing the anisotropy of the scattering. These quantities depend on the particulate loading as well as the distributions of the size and optical properties of the particles.

For a spherical particle of homogeneous, optically isotropic material, characterized by a complex refractive index $m \equiv (n - ik)$ Mie theory allows one to compute the spectral absorption ($Q_{\lambda,a}$) and scattering ($Q_{\lambda,s}$) efficiencies of the particle, as well as the phase function ϕ_λ. For randomly polarized radiation, these quantities are a function of the particle size parameter $x \equiv (\pi d/\lambda)$, and the complex refractive index $m(C, \lambda, T)$, a function of composition, wavelength and temperature.

For a monodispersion of identical spherical particles, of specified loading (i.e. number density), the particulate's contribution to the optical properties (a_λ, σ_λ and Φ_λ) of the medium are simply related to the spectral properties ($Q_{\lambda,a}$, $Q_{\lambda,s}$, ϕ_λ) of a single particle. It is also straightforward to compute the spectral optical properties of the medium for a polydispersion of spheres of identical composition, by convolving the results of Mie calculations for spheres of varying diameter (i.e. x) for fixed wavelength (and hence fixed m), with the particle size distribution (assumed given). In the case of a particulate material, like flyash, for which it is reasonable to assume that individual particles are of homogeneous composition but the composition varies from particle to particle, it is still possible to compute the spectral characteristics of the particulate dispersion by dividing the particles into an appropriate number of classes of varying composition (and hence m), each having a specified size distribution, and summing over particle classes.

In radiative heat transfer calculations, the contribution of the gas to the spectral absorption coefficient is added to that of the particles to obtain the combined optical properties of the medium on a spectral basis. These optical properties are then used as input for a radiation transfer code to calculate radiative fluxes, on a spectral basis, for a particular combustor geometry and boundary conditions. Finally, to obtain total heat transfer quantities such as the overall radiant heat flux, integrations over wavelength must be made.

The procedure, outlined above, represents the only logical approach to the computation of radiative heat transfer in flyash laden combustion gases. To implement this procedure requires, as input, a detailed characterization of the ash with respect to its size and (complex) refractive index distributions on a spectral basis.

Now, while techniques are available for determining the size distribution of powder samples, such as flyash, there are no practical means available for reliably determining the complex refractive index distribution of a complex material such as flyash either on a single particle basis, as a powder or as a dispersed aerosol. However, it is possible, using modern microanalytical techniques, specifically computer-automated SEM/EDX analysis, to determine the size and chemical composition of a heterogeneous powder on a particle by particle basis for a statistically large number of particles.

If the compositions of individual particles can be related to the complex refractive index of their material, then the characterization of a particular ash in terms of its size and composition distributions can lead to the necessary input for carrying out the calculations, outlined above, to compute radiation transfer in combustion systems containing that ash.

Thus the key requirement, necessary for the implementation of this approach, is data on the optical constants (i.e. the components n, k of the complex refractive index) as a function of composition, wavelength and temperature covering the range of compositions found in representative ashes. Since, as noted above, and emphasized in texts on the optical properties of particulate matter, it is impractical to extract reliable data on the optical constants of material in particulate form, the only viable approach is to make measurements on homogeneous bulk samples for which well-established techniques are available.

The foregoing arguments provide the rationale for the present program. Characterization of representative flyashes concerning their size and composition distributions constitutes Task 1, while measurements of the optical constants on bulk samples of synthetic slags as a function of relevant ranges of composition, wavelength and temperature constitute Task 2. Task 3 is designed to provide computational capabilities to support the other tasks, while Task 4 is planned to provide an experimental test that the measured optical properties of a dispersion of flyash can indeed be computed reliably from a knowledge of the size and composition distributions of the ash.

1.2 Description of Tasks

TASK 1 - Characterization of Flyash

Extensive prior analyses of flyash from a wide range of coals plus analyses of the mineral matter in raw coals, together with knowledge of the transformation processes occurring during combustion, lead to the following overall picture of the nature of flyash.

The particle size distribution is very broad with a volume (or mass) mean diameter on the order of 10 μm. Typically it is well represented by a log normal distribution with the 1% and 99% sizes in a cumulative plot by volume occurring at ~1 μm and 70 μm respectively. Evidence of a distinct submicron fume due to homogeneous condensation of volatile mineral matter is sometimes found, but this fraction can be expected to contribute negligibly to radiation transfer.

With regard to chemical composition, several distinct classes of particle can be identified and plausibly related to their origin and formation mechanisms.

By far the preponderant class, usually representing on the order of 90% or more of the ash on a mass basis, consists of vitreous (amorphous) material composed primarily of SiO_2, Al_2O_3, CaO and MgO, usually in that order, but containing varying smaller percentages of other metal oxides, notably Fe_2O_3. It can appropriately be identified as particles of impure (calcium) aluminosilicate glass derived from the microscopic clay-like mineral inclusions in the coal matrix. As char burnout proceeds these inclusions melt and form liquid globules on the surface of the char (which they do not wet) and are then released into the gas.

These glassy particles tend to be quite spherical with smooth surfaces and of reasonably homogeneous composition as is to be expected from their formation as liquid droplets. As they cool after release from the char surface, they remain in the vitreous state because the cooling rate is much faster than the crystallization rate for the formation of specific phases. The fact that the bulk of most ashes consists of reasonably spherical, homogeneous and vitreous (and therefore optically isotropic) particles is a very fortunate fact, since they satisfy the assumptions of the Mie theory remarkably well.

Micrographs of optically polished sections of ash cast in epoxy resin, shows that these glassy particles sometimes contain a number of small bubbles of gas evolved from the char and trapped in the particles as they form on the char surface. More rarely, large, thin-walled cenospheres are observed which presumably are "glass-blown" when a liquid drop covers a pore in the char from which a relatively large volume of gas is evolved under pressure. Although such cenospheres are very prominent objects in micrographs, their number is usually too small to significantly affect radiation transfer.

Auger spectroscopic studies of ash often show a thin surface layer composed of volatile metals and high in sulfur (as sulfates) and water. The presence of a thin layer of adsorbed water containing sulfate ions controls the electrical resistance of the surface which is very important in the performance of electrostatic precipitators. However, this surface layer, of different composition from the underlying particle, is too thin (≤100Å) relative to wavelengths of interest to affect the optical properties of the particle.

Apart from this major class of glassy particles, several distinct minor classes of particle types can be identified, each comprising, at most, a few percent by mass of the flyash. One such class consists of incompletely burned char particles which are clearly identified in optical and SEM micrographs by the fact that they are black, of irregular shape and porous. The mass fraction of char depends on the particular coal and the combustor configuration and operating conditions. In modern combustors the mass fraction of unburned char is normally a few percent at most.

Another minor class consists of particles of adventitious incombustible mineral matter (e.g. quartz) which is contained in the pulverized coal feed. Such particles are usually large and of irregular shape, often showing rounded edges indicating partial melting.

A third minor class consists of magnetite (Fe_3O_4) which derives from the combustion of pyrite (FeS_2) particles contained in the coal grind. These magnetite particles are black, generally spherical, magnetic and much denser than the glassy particles. The proportion of magnetite particles depends on the coal type, being largest in high sulfur coals, because the sulfur is mostly associated with pyrite. Recent work has shown that much of the pyrite in the coal grind can be removed by washing/sedimentation with a reduction in SO_x emissions as high as 50% in some high sulfur coals.

The ashes selected for characterization are samples from power plants or pilot-scale combustors derived from the same seven coals selected for study under the parallel PETC program on "Transformation of Inorganic Coal Constituents in Combustion Systems" which comprise four bituminous, one sub-bituminous and two lignite coals.

A variety of techniques are being used in the characterization of these ashes. The principal method for determining size distributions employs a Coulter Multisizer which is capable of giving accurate, reliable results of high resolution over a wide dynamic range ≤1 μm to ≥ 100 μm.

Automated, computer-controlled, combined SEM/EDX microanalysis will be the principal technique used to determine the distributions of composition and size for a large number (~1000) of particles for each ash. The size distributions will be compared with those obtained by the Coulter counter.

Other techniques to be used include classification by density using liquids of varying density in a centrifuge, together with classification by size using a wet-sieving method. These techniques can yield density and size separated fractions for further examination by microanalytical techniques such as energy-dispersive X-ray spectroscopy. In addition, the magnetite particles may be separated by magnetic separation. The char content will be determined by low temperature ashing.

TASK 2 - Measurements of Optical Constants of Synthetic Slags

This task is planned to provide the basic optical properties data in a comprehensive and conveniently usable form. The optical constants (i.e., the components of the complex refractive index $m = n - ik$) of samples of synthetic slags of controlled compositions will be measured using established techniques involving transmission and surface reflectance methods. The wavelength range will extend from the visible to 12 μm, and the temperature range will extend to 2000K.

In earlier work at Stanford, supported by NSF, extensive measurements of this type were made on polished wafers of synthetic slags at temperatures up to 1200 K. A major component of this task will be to extend such measurements to higher temperatures (~2000 K) where the slag is liquid. This requires the development of modified techniques which present a number of more or less severe technical challenges.

Initially, the optical constants of the basic calcium-aluminosilicate host glass will be determined for the composition range defined by Task 1. Subsequently, by adding infrared-active mineral oxide constituents in controlled amounts, one at a time, the modifications to $m(\lambda, T)$ produced by such constituents will be quantitatively determined. The particular constituents (and their range of mass fractions) to be examined will be determined by those disclosed by Task 1, taking account of knowledge of the optical activity at relevant wavelengths of such additions from the literature of glass technology. Specific constituents to be examined will include Fe_2O_3, taking especial account of its valence state (Fe^{2+}/Fe^{3+} ratio), and of TiO_2. The contribution of the OH radical to the optical properties will be evaluated and quantified if significant.

The experimental data on $m(\lambda, T)$ as a function of composition, over the range relevant to coal ashes, will be reduced to generate simple correlation formulae. The latter will constitute the data base necessary to calculate the radiative properties of bulk slags and ash dispersions required for understanding and computing radiative transfer in coal combustion systems.

TASK 3 - Sample Calculations of the Radiant Properties of Flyash Dispersions

This task is intended to provide computational capabilities to support the other tasks. It includes the following components.

(i) A Mie scattering code to calculate the absorption and scattering efficiencies and phase function of a single sphere of specified size parameter and complex refractive index. A modified Mie code will also allow such computations for hollow spheres.

(ii) A code to convolve the results from (i) over a specified size distribution and loading to compute the absorption and scattering coefficients and phase function of a homogeneous polydispersion.

(iii) A code to sum the results of (ii) for a number of classes of particles of varying refractive indices and size distributions, i.e. for a heterogeneous polydispersion.

(iv) A radiation transfer code to calculate the absorption, scattering and emission characteristics of a homogenous, isothermal slab of dispersed ash on a spectral basis.

(v) A code to integrate the spectral results from (iv) over wavelength to yield the total radiative properties of the slab.

Calculations using these codes will be used to provide sensitivity analyses to guide the characterization work of Task 1, and to design and evaluate the results of Task 4.

TASK 4 - Measurement of the Radiative Properties of Flyash Dispersions

The purpose of this laboratory scale experiment is to test our ability to predict the measured radiative properties of a dispersion of well-characterized flyash. As such it will provide a critical test of the effectiveness of the overall approach adopted in this program.

2.0 PROGRESS IN THE PAST QUARTER

2.1 Task 1: Characterization of Flyash

2.1.1 Density Classification

The process of density classification by centrifugal separation is now complete. The results are shown in Table I.

TABLE I

DENSITY CLASSIFICATION OF REPRESENTATIVE FLYASHES

(All Numbers are Percentages by Mass)

Flyash	<1.6 g/cc	1.6–2.0 g/cc	2.0–2.4 g/cc	2.4–2.8 g/cc	2.8–3.2 g/cc	>3.2 g/cc
Kentucky #9 (Baghouse)	0.94	7.62	26.69	59.63	1.38	3.74
Kentucky #9 (Cyclone)	2.46	11.84	39.27	35.06	4.01	7.37
Illinois #6 (Baghouse)	1.25	7.20	42.78	41.98	2.82	3.97
Illinois #6 (Cyclone)	0.72	5.05	33.0	50.44	2.82	7.97
Beulah (Baghouse)	0.23	2.10	10.21	76.28	8.90	2.28
Beulah (Cyclone)	2.73	5.37	28.26	57.01	2.65	3.99
Upper Freeport	1.27	6.70	26.97	57.06	2.37	5.63
San Miguel	35.60	52.86	7.05	3.52	0.97	---
Eagle Butte	0.50	0.24	3.45	21.42	68.49	5.90

For all but two ashes, it appears that 80% or more of the ash by mass is in the density range 2.0-2.8 g/cc. Of the two prominent exceptions, the Texas lignite fly ash from San Miguel has 90% of its mass in the density range < 1.6-2.0 g/cc. This indicates that a large fraction of the flyash in this category consists of cenospheres (particles containing bubbles). This will be confirmed by examining polished sections of ash particles embedded in a matrix of epoxy. The other exception is the flyash from the Eagle Butte subbituminous coal. More than two-thirds of this ash falls in the density category 2.8-3.2 g/cc; probably due to relatively higher alumina and calcia content.

2.1.2 Microanalysis by SEM/EDX

As reported in the last QPR, samples of flyashes from Kentucky #9, Illinois #6 and Upper Freeport coals were sent to the University of North Dakota Energy Research Center (UNDERC) for computer controlled scanning electron microanalysis (CCSEM) examination on a particle-by-particle basis. The well deagglomerated SEM samples were prepared at Stanford. The results have since been received and the data analyzed.

Figures 1, 2 and 3 show size distributions obtained from CCSEM data compared with results from Coulter Multisizer analyses. For the Upper Freeport ash, the data is also compared with that previously obtained on a sample prepared at UNDERC. The CCSEM data show log-normal behavior since they plot as a straight line, with a slope (i.e., the geometric standard deviation) close to that corresponding to the Multisizer data. However, the median diameter for the former distribution is about 50% larger than the latter for all ashes. Similar discrepancies were found for the other three ashes (from Illinois #6, Kentucky #9 and Beulah coals) as reported in the last QPR.

In Figure 3, it is observed that the size distributions arising from the SEM data from the two samples are very close. Thus, even with relatively well deagglomerated samples, there appears to be a deficiency of small ash particles – when compared with the results from the Coulter Multisizer. We are planning tests to determine the explanation for this discrepancy. One test involves the CCSEM sizing of a bimodal sample prepared using nominally monosize glass microspheres that are commercially available. The results should indicate why fewer of the smaller particles are being detected by the electron beam.

Figure 4 shows the average elemental composition of the three ashes represented on an undersize basis. This means the y-axis shows the percentage by mass of the element averaged for all ash particles below a given size (in microns) corresponding to the x-axis value. The number fraction undersize irrespective of composition is also plotted for each flyash. The elements selected are the four major constituents and iron. Both the new and the old data for the Upper Freeport ashes are shown.

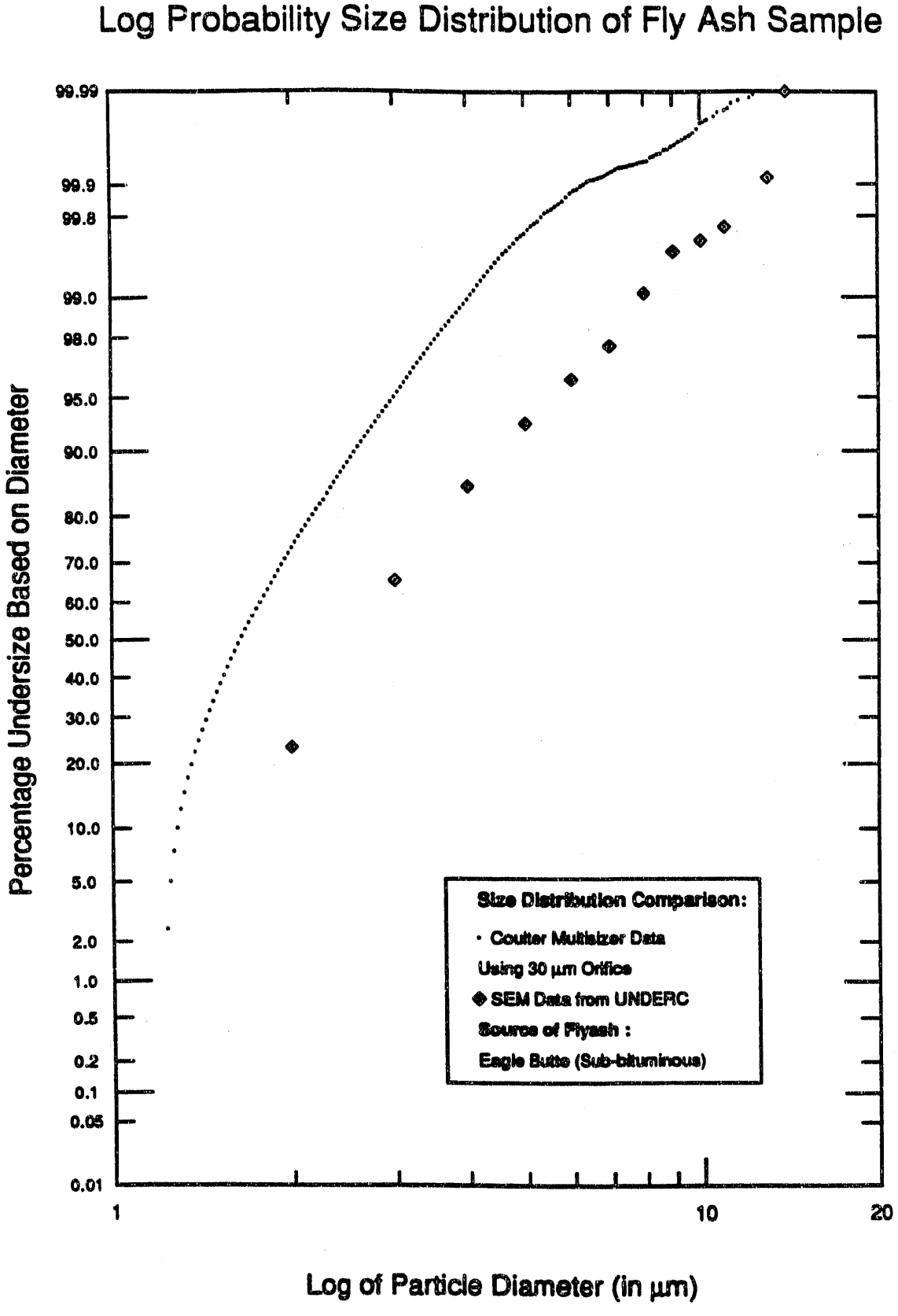

Figure 1. Size distribution of Eagle Butte coal fly ash.

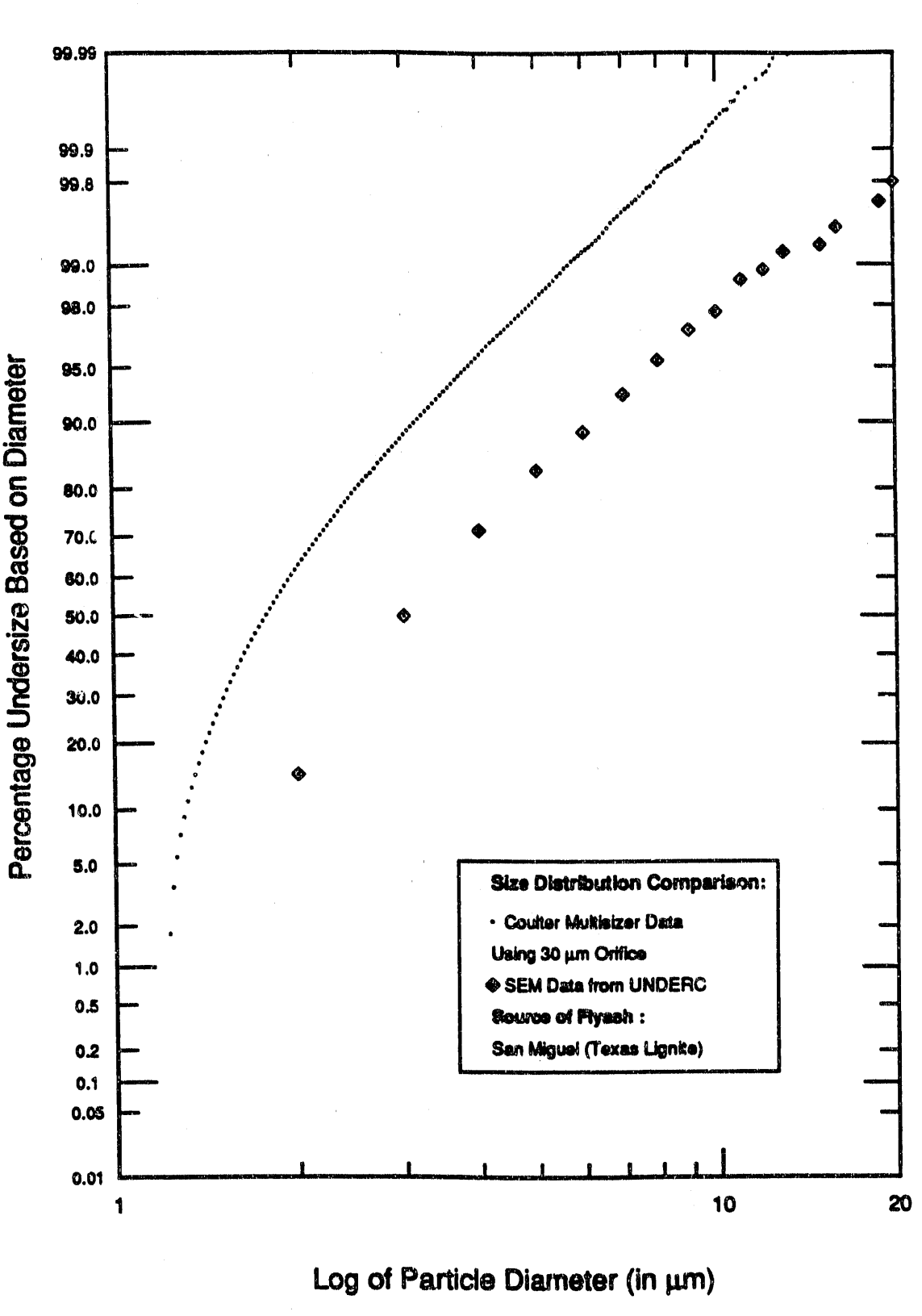

Figure 2. Size distribution of San Miguel coal fly ash.

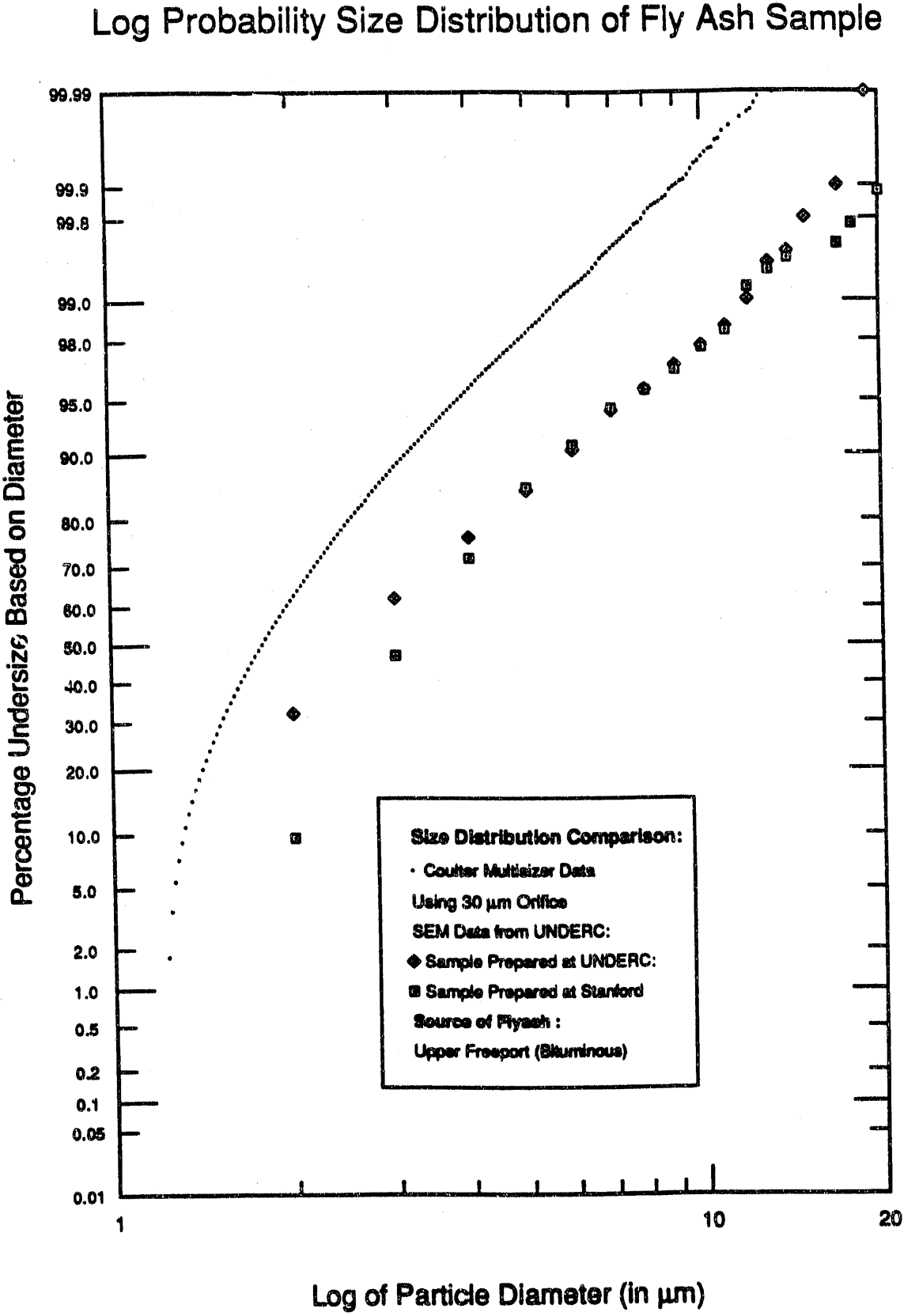

Figure 3. Size distribution of Upper Freeport coal.

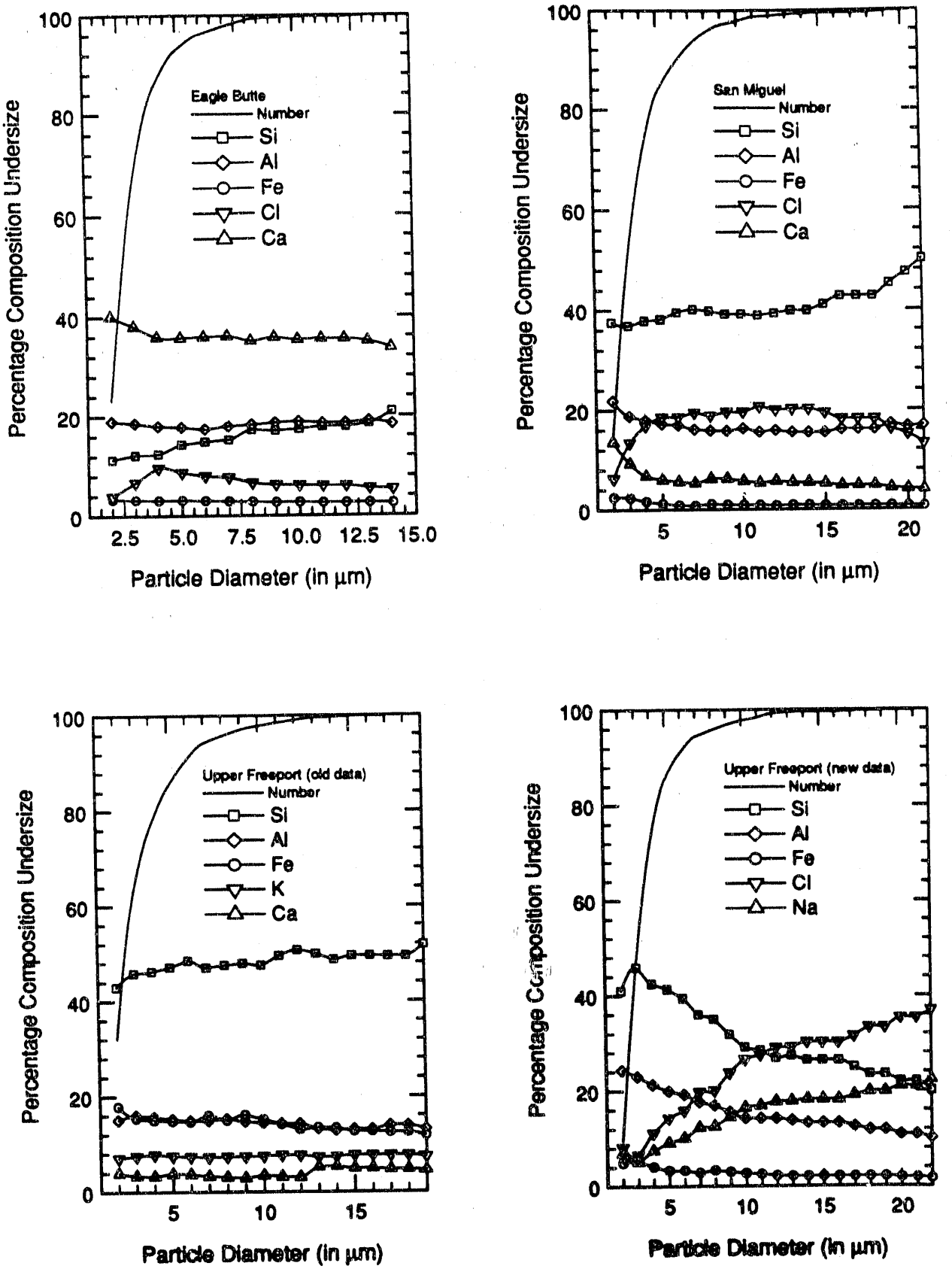

Figure 4. Average elemental composition of flyash particles from CCSEM analysis.

An unexpected result is the high chlorine content of all three ashes and the high sodium content of the Upper Freeport ash. The latter was not seen in the previous analysis. It seems unlikely that the ashes actually contain such high proportions of these two elements and it is possible that the samples may have become contaminated by sodium chloride inadvertently during sample preparation. This will be checked by preparing new samples for analysis. Also, microprobe analysis of bulk slag samples prepared by melting the whole ashes (see next section) should help resolve this question.

The two analyses of the Upper Freeport ashes differ primarily in the much higher sodium and chlorine content of the newer analysis. Consequently, the percentage contributions by the other elements has decreased significantly – especially iron. The distribution of silicon shows opposing trends in the two analyses – showing a greater concentration in the smaller particles in the newer analysis. Aluminum behaves similarly – unlike the first analysis where it showed little variation with particle size.

The Eagle Butte ash is unusual because calcium, rather than silicon, is its single largest constituent. This is the reason for its high density. The Eagle Butte ash is also the only one with an average silicon to aluminum ratio close to unity. For other ashes, this ratio is closer to 2:1. The silicon in both the San Miguel and Eagle Butte ashes are present in slightly higher proportions in the larger particles. They have a rather low iron content – which appear to be distributed evenly among particles of different sizes. Smaller San Miguel ash particles contain higher proportion of calcium.

Figure 5 shows ternary plots for the three fly ashes. (See previous QPR for a more detailed discussion of ternary plots.) The "center of gravity" of the Eagle Butte ash is shifted towards the "Other" vertex because of its high non-aluminosilicate content. The particles that lie on the sides of the triangle are devoid of either aluminum or silicon. The other two ashes have a high concentration of particles at the "Other" vertex corresponding to the high sodium and chlorine detected in many particles. There are very few iron-rich particles in the three ashes.

We now have CCSEM data for all six ashes and will continue to analyze them during the next quarter.

2.1.2 Electron Microprobe Analysis for the Bulk Composition of Flyash

An accurate knowledge of the bulk composition of the six flyashes is necessary for many reasons – ranging from a comparison of the data with the average composition obtained from the CCSEM data, to determining the fraction of iron present as magnetite. Slag samples have been prepared by melting each ash in alumina crucibles. Polished samples will be prepared from these slags which will then be analyzed using electron microprobe.

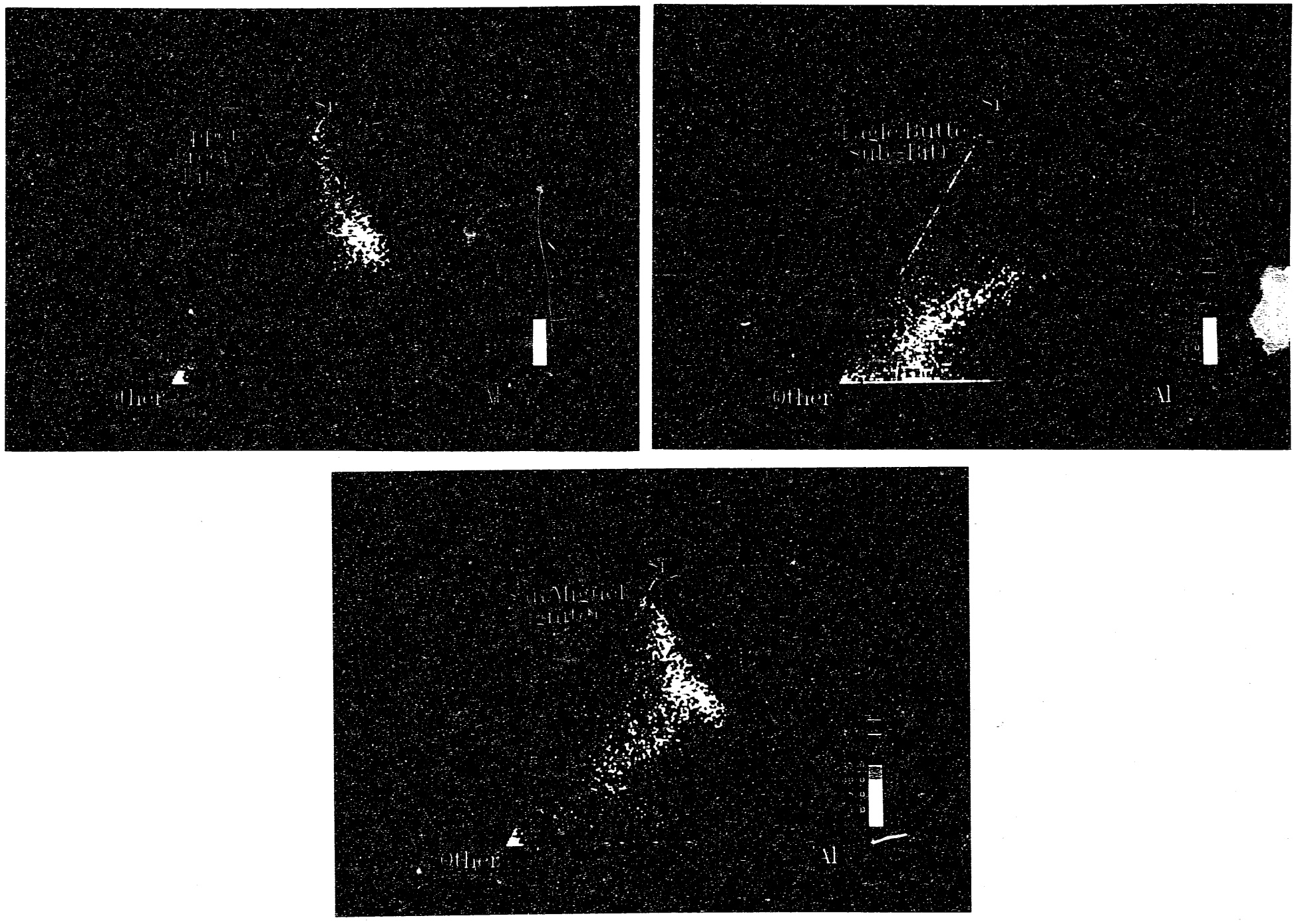

Figure 5. Ternary Composition Diagrams from CCSEM/EDX Analyses.

2.2 Task 2: Optical Properties of High Temperature Slag

The immediate goal of this task is to measure the high temperature optical properties of coal slag. The complex refractive index, $m = n - ik$, will be measured for synthetic slags at temperatures near 1900 K. The effect of composition on the optical properties will be investigated.

As established in the earlier work of Goodwin on solid slag samples, two separate techniques are required to determine n and k over the whole wavelength range from the visible to $\lambda \sim 12\ \mu m$ For $\lambda \leq 5\ \mu m$, where k is small enough ($< 10^{-2}$) that the transmission T of a thin, optically polished wafer (thickness h) is not too small to allow accurate measurement, the absorption index, k, can be found from the formula

$$T = exp(-4\pi kh/\lambda) \tag{1}$$

When k is known, the real index, n, can be found from measurement of the near normal reflectance, R_n, using the Fresnel formula

$$R_n = \frac{(n-1)^2 + k^2}{(n+1)^2 + k^2} \tag{2}$$

For $\lambda < 5\ \mu m$, n can be found from the measured values of R_n using Eq.(2) with the values of k determined from the measured values of T using Eq.(1).

For $\lambda \geq 5\ \mu m$, where k is too large to allow transmittance measurements, values of n and k may both be inferred solely from reflectance measurements (provided they are made over a large enough wavelength range) by use of the Kramers-Kronig relations which are analytic formulas relating n and k in integral forms. The Kramers-Kronig relations are

$$n(\omega) - 1 = \frac{2}{\pi} P \int_0^\infty \frac{\omega' k(\omega')}{\omega'^2 - \omega^2} d\omega' \tag{3}$$

and

$$k(\omega) = -\frac{2}{\pi} P \int_0^\infty \frac{n(\omega')}{\omega'^2 - \omega^2} d\omega' \tag{4}$$

where ω is frequency and P denotes the Cauchy principal values of the integrals.

For high temperatures, when the slag is molten, the same two basic methods may be used, but the experimental techniques must be modified. Also, since the measurements mus' be made with the sample inside a high temperature furnace, considerable technical difficulties must be overcome.

To measure the absorption index, we are using a "submerged reflector" technique whereby a platinum mirror is suspended just below the liquid surface and the absorption index is measured by a double pass through the thin, overlying slag layer. By measuring the change in absorption when the mirror is displaced by a small increment Δh, the absorption index can be found from the change in transmission from the formula

$$\frac{T_{h+\Delta h}}{T_h} = exp\left(-\frac{4\pi k(2\Delta h)}{\lambda}\right) \tag{5}$$

without having to know the reflectivity of the platinum mirror.

As reported in a previous QPR, we have successfully implemented this technique and made measurements of k on a molten synthetic slag containing 5% Fe_2O_3 (SA05) at 1600°C over the range $1 \leq \lambda \leq 5\ \mu m$. The measurements are in accord with those of Goodwin on slag of the same composition at lower temperatures.

During the last quarter, the near normal reflectance measurement technique has been successfully implemented and measurements were made for three different synthetic slag compositions. Several improvements to the optical system were necessary before accurate measurements could be made.

Improved Optical System

An improved optical system was designed and constructed during the past quarter to eliminate several problems. Figure 6 shows a schematic of this new design. Two basic improvements were made: 1) the mirror above the furnace, M4, and the gold reference mirror were repositioned to eliminate errors due to contamination of mirror M4, and 2) the Nernst glower image was rotated 90 degrees to allow optical realignment to be accomplished more rapidly.

As reported in the last QPR, when performing near normal reflectance measurements, the mirror above the furnace opening (M4) becomes contaminated during the measurements. Hot vapors, probably from the binders in the insulation and/or high temperature adhesives in the furnace, condense on mirror M4. In the previous optical design, reflectance

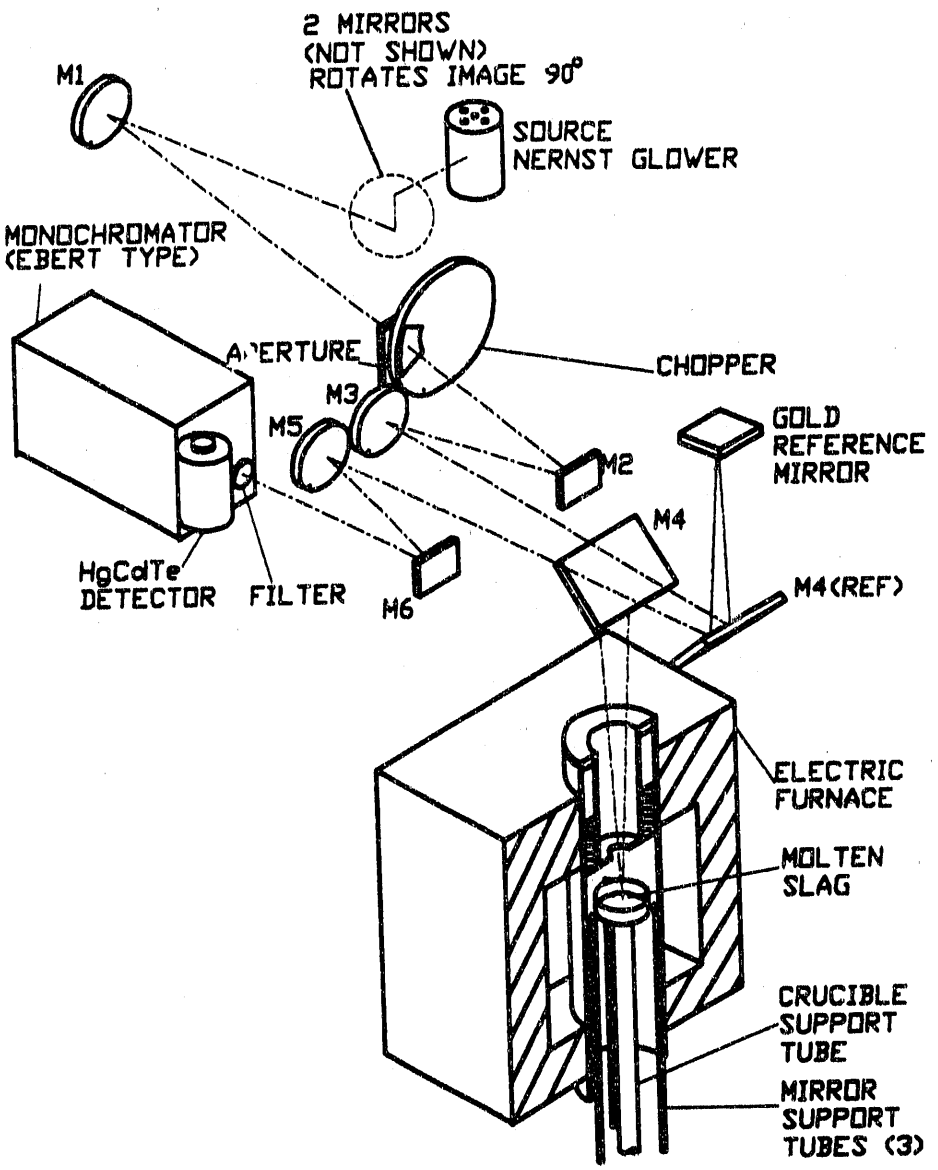

Figure 6. Schematic of the optical system for high temperature reflectance measurements.

measurements were made by placing M4 into the optical path to collect the sample signal and removing M4 from the path to obtain a reference signal; therefore, once the mirror M4 is contaminated, low reflectance values are measured. Since the contamination accumulates during the experiment, we are unable to correct the error.

In the new design, the mirror M4 is always in the optical path, but by moving it from one position to another, we are able to obtain the sample and reference signals. The mirror still becomes contaminated by vapors from the furnace, but both paths show the same diminished signal and thus the effect is cancelled as we take the ratio sample/reference to obtain the reflectance. Care is taken to not allow the mirror to dwell above the furnace any longer than necessary, so that the contamination can be minimized.

To be assured that the contamination is cancelled by the new arrangement, the reflectance of a gold mirror is measured both before and after a reflectance measurement of slag. No significant difference was measured in any of the experiments thus far, despite the visible degradation of the reflectivity of the gold mirror M4. Apparently the contamination is fairly uniform over the active region of the gold mirror.

The second improvement, the rotation of the Nernst glower image, has proven to be only minor. It was reported in the last QPR that the optical system had to be carefully aligned at each wavelength for both the reference and sample paths. Since the slits on the monochromator are vertical, it was hoped that by having a horizontal image on the vertical slits, any slight horizontal misalignment would be negligible, since from previous measurements the misalignment seemed to be horizontal. The new arrangement does improve the situation, and alignment can now be done more quickly, but now the misalignment from wavelength to wavelength is chiefly vertical. This switch from horizontal to vertical misalignment indicates the problem is due to nonuniformity of the glower image across its narrow dimension (2 mm). Other minor changes to the optical system have not corrected the problem.

Fortunately, this sensitivity to alignment does not hinder progress, since we are capable of measuring reflectance very precisely provided we carefully align the mirror M6 to maximize the signal at each wavelength.

Reflectance Measurements

During the past quarter, reflectance measurements were made for synthetic slags SA00 (weight percentage composition ~58% SiO_2, 29% CaO, and 13% Al_2O_3), SA01 (SA00 + 1% Fe_2O_3), and SA05 (SA00 + 5% Fe_2O_3) at 1600°C. For each of the three slags, the following procedures were used to obtain the reflectance over the wavelength range from 1 to 13 μm.

Before heating the furnace, the optics are aligned for near normal reflectance measurements using a mixture of water and graphite. The graphite causes any light that penetrates the liquid surface to be absorbed. Once the furnace position is aligned using water in the sample position, more precise alignment is done by replacing the water with a gold mirror. This measurement allows detection of minor misalignments since we know the reflectivity of the gold mirror is close to unity.

Next the gold mirror is removed and a metal hood is sealed over the entire optical system while it is purged with nitrogen. By purging the system with nitrogen, the infrared active gases (chiefly CO_2 and H_2O) are removed and the transmittance of the hot column of gas in the furnace is identical to that of the cool exterior gas. The purging continues for 8-12 hours or until no CO_2 is detected near its 4.3 μm absorption band.

Once the purge is complete, 20-30 ml of slag (small chips from a previously made melt) is placed in a 50 ml alumina crucible inside the furnace. The furnace is heated at about 10°C per minute until the furnace reaches 1600°C. The furnace is held at that temperature for 1-2 hours while the optics is aligned. The reflectance is carefully checked to see that it is constant over a period of about an hour, indicating that the molten slag surface is clean and smooth.

With the molten slag surface and the optics aligned, reflectance measurements proceed. To measure the reflectance, the mirror M4 is placed over the furnace, collecting the surface reflection, and the monochromator is set to the first wavelength. The detector signal is measured with the lock-in amplifier and the monochromator is re-set to the next wavelength. After the sample path signal has been recorded at 4 or 5 wavelengths, mirror M4 is moved to its reference position and the signal is recorded for the same 4 or 5 wavelengths. Mirror M6 is adjusted slightly between each measurement to ensure that the signal is maximized. After the 4 or 5 reference signals have been recorded, M4 is placed back into the sample position to check that the signals did not drift over the time required for the 4 or 5 measurements. This whole procedure is then repeated for the next wavelength interval until the whole range has been covered.

Once the reflectance is measured for the entire wavelength range, the furnace is cooled and the slag is saved for composition analysis.

Reflectance Results

The reflectance data in the wavelength range 1-13 μm are shown in Figure 7. Initially, data were collected over the wavelength range 1-14 μm, but for wavelengths larger than 13 μm, the signal is so small (≤ 100 μV) that a large time constant (10 seconds or more) is

required on the lock-in amplifier to reduce the noise to an acceptable level. For such large time constants, it is not possible to adjust the optics since the integration time causes large delays between adjustment and response by the detector. Since failure to maximize the signal has been shown (see previous QPR) to produce erroneous results, we reject data at wavelengths greater than 13 μm where the signals are very weak. Unfortunately, the lack of data beyond 13 μm increases the uncertainty in the computed absorption index, k, at long wavelengths.

Note that the signals are weak at these long wavelengths for a number of reasons, unrelated to the optical properties of the slag. Namely, the power from the thermal broadband source (Nernst glower) decreases with increasing wavelength, the efficiency of the monochromator grating decreases as one tunes away from the blaze wavelength (10 μm), and the spectral responsivity R_λ of the Mercury-Cadmium-Telluride detector decreases sharply beyond 12 μm ($R_{13\mu m}/R_{12\mu m} < 50\%$ and $R_{14\mu m}/R_{12\mu m} < 15\%$).

The measured reflectance shown in Fig. 7 has the expected qualitative behavior over the entire wavelength range. Near 1 μm, the reflectance is approximately 4.5%. It decreases as wavelength increases until it reaches a minimum (but non-zero) near 8 μm. The reflectance increases sharply past 8 μm to a maximum of approximately 15% at 9.5-10 μm before decreasing. The higher iron slag, SA05, has a slightly smaller maximum of approximately 13.5%. The reflectance of the other two slags, SA00 and SA01, are not significantly different except at the longest wavelengths where the reflectance increases slightly with increasing iron content.

Also shown on Figure 7 is the reflectance of slag SA05 at room temperature. It is clear that there is a significant difference between the near normal reflectance at room temperature and that at 1600°C. In the wavelength range below 6 or 7 μm the reflectance at high temperature is not significantly different from that at low temperature. Near 8 μm both the high and low temperature slags have a minimum reflectance, but the minimum occurs at longer wavelengths in the high temperature slags. At wavelengths above 8 μm there is a noticeable difference between the reflectance of high and low temperature slag.

Figure 8 shows the measured reflectance on a logarithmic scale to show more clearly the effect of temperature on the minimum reflectance. The high temperature slag has a minimum reflectance of approximately 0.3% while the low temperature slag has a minimum nearer 0.07%. Low temperature measurements on other slags show similar trends.

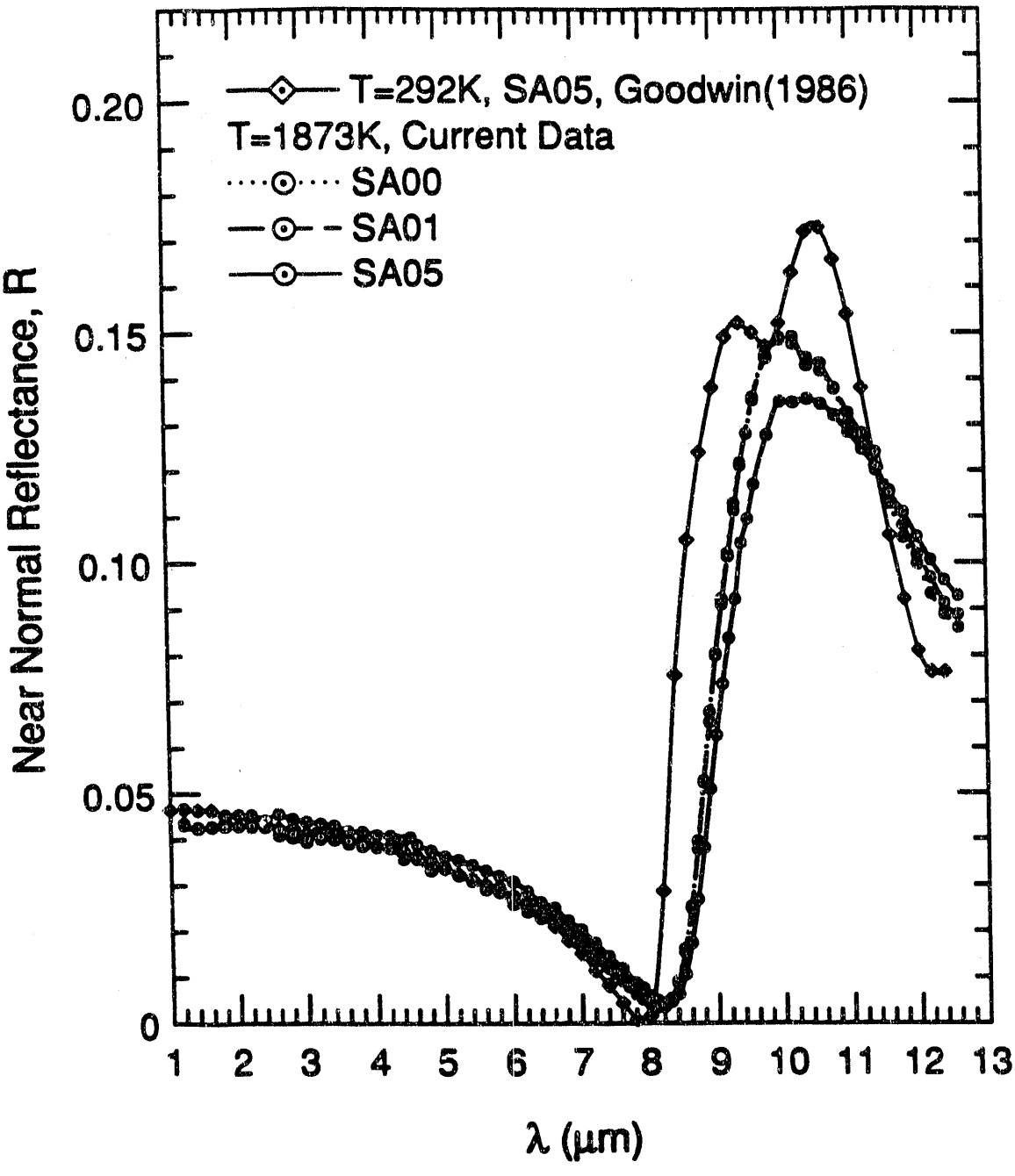

Figure 7. The near normal reflectance for molten synthetic slags SA00, SA01, and SA05 at 1600°C.

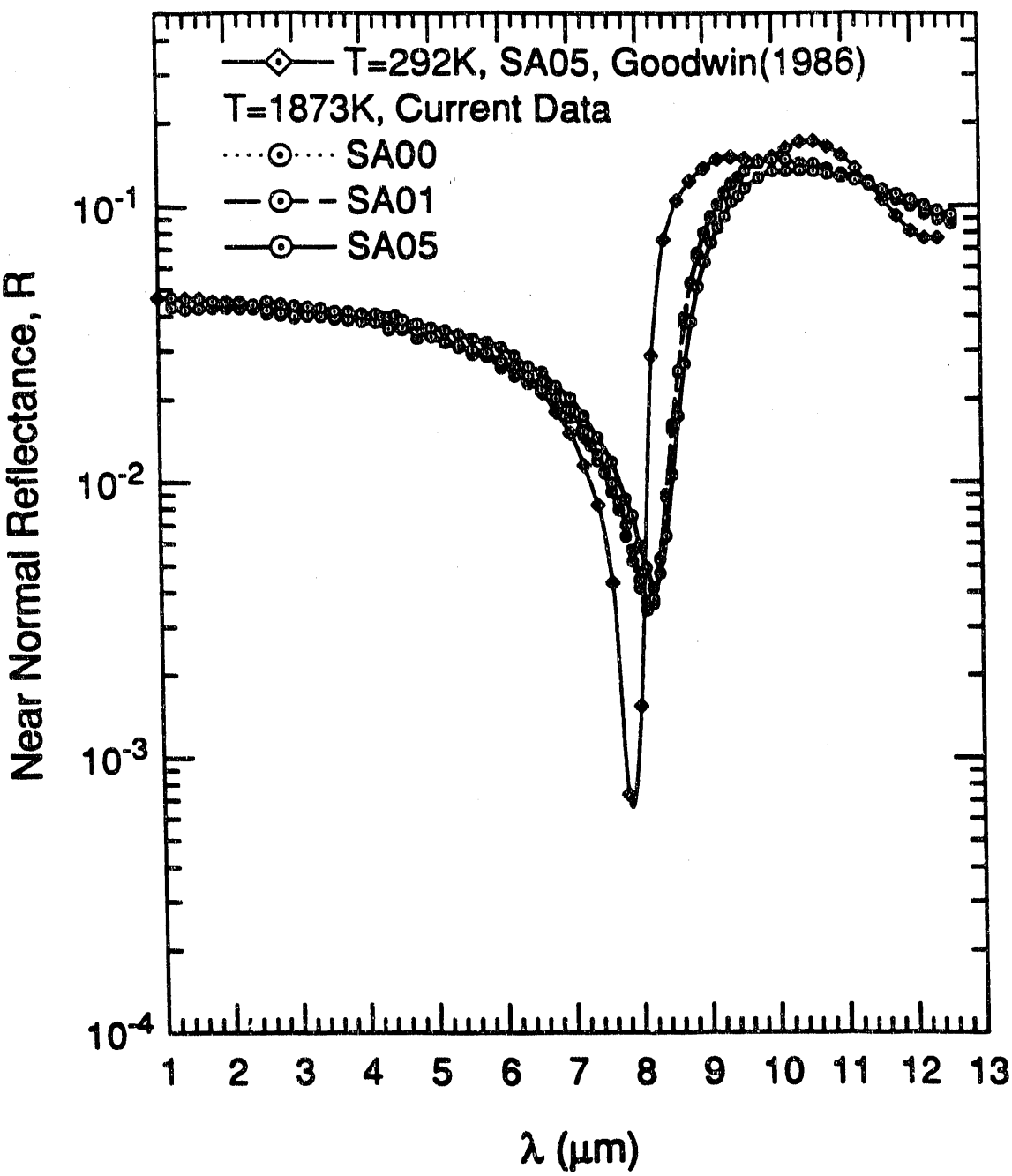

Figure 8. The near normal reflectance for molten synthetic slags SA00, SA01, and SA05 at 1600°C and for the room temperature slag SA05.

Data Reduction and the Kramers-Kronig Analysis

The Kramers-Kronig relations were utilized to reduce the near normal reflectance data to yield n and k. The general statement of the relationships between n and k expressed in Eq. (3-4) are not in a particularly useful form. Instead, the form of the Kramers-Kronig relations used here are in terms of a reflection coefficient r and phase shift on reflection θ_R. The reflection coefficient r is related to the reflectance by $R_n = |r|^2$ and the phase shift is defined as $r = |r|\exp(i\theta_R)$. In this form we have

$$\theta_R(\omega) - \pi = -\frac{\omega}{\pi} P \int_0^\infty \frac{ln\, R_n(\omega')}{\omega'^2 - \omega^2} d\omega' \tag{6}$$

Once $\theta_R(w)$ is computed using a sufficiently wide wavelength range of reflectance data, n and k are computed using the relations

$$n = \frac{1 - R_n}{1 + R_n + 2\sqrt{R_n}\cos\theta_R} \tag{7}$$

$$k = \frac{-2\sqrt{R_n}\sin\theta_R}{1 + R_n + 2\sqrt{R_n}\cos\theta_R} \tag{8}$$

Note here that $\theta_R - \pi$ is small when k is small so that Eq. (7) is a restatement of the Fresnel relation, Eq. (2), for $k << (n - 1)$. This leads to the conclusion that the KK relations may be used to compute n outside the range for which they may be used to compute k.

The integral shown in equation (6) can be evaluated analytically outside the wavelength range for which we have data by assuming the reflectance is constant outside the range of available data. That is, assuming

$$R_n(\omega) = R_n(\omega_a), (\omega \leq \omega_a) \tag{9a}$$

$$R_n(\omega) = R_n(\omega_b), (\omega \geq \omega_b) \tag{9b}$$

where $w_a \leq w_b$ is the frequency range of the available reflectance data By subtracting $lnR_n(w)/(w'^2-w^2)$ from the integrand of Eq. (6), which is allowed since $\int_0^\infty 1/(w'^2-w^2)$ the integrand becomes finite and can be computed easily. The resulting expression for the phase shift is

$$\theta_R(\omega) - \pi = \frac{ln(R_n(\omega_a)/R_n(\omega))}{2\pi} ln|\frac{\omega+\omega_a}{\omega-\omega_a}| + \frac{ln(R_n(\omega_b)/R_n(\omega_b))}{2\pi} ln|\frac{\omega_b-\omega}{\omega_b+\omega}| - \frac{\omega}{\pi}\int_{\omega_a}^{\omega_b} \frac{ln\,R_n(\omega') - ln\,R_n(\omega)}{\omega'^2-\omega^2} d\omega' \quad (10)$$

The assumption that variations in the reflectance outside of the measured wavelength range are not important is critical to the data reduction to follow. By making this assumption, we assume that there are not strong absorption mechanisms just beyond the end points of the measurement wavelength interval.

A computer program was written to compute n and k using the above relations. The integral in Eq. (10) is readily computed using a simple trapezoid approximation. Higher order integration schemes were tested but, given the wavelength resolution of the measurements, were found to give identical results within the experimental uncertainty.

The KK method described above gives n accurately over the entire wavelength range 1-13 μm but can only be used to determine k at wavelengths where $k > 0.1$. This limitation to larger k values is easily explained by referring to the Fresnel relation (Eq. (2)). When k is small compared to $n-1$, the reflectance, R, is very weakly dependent on k. If k is small but $n-1$ is much smaller, for example, at the wavelengths at which $n = 1$, the normal reflectance is simply

$$R_{n=1} = \frac{k^2}{k^2+4} \quad (11)$$

so that

$$k_{n=1} = \frac{4R}{1-R} \quad (12)$$

Unfortunately, for the high temperature slags the wavelength where $n = 1$ lies well into the SiO_2 restrahlen absorption band and $k_{n=1} > 0.1$. Therefore, Eq. (12) offers no new information, but calculating k using Eq. (12) agreed with the KK analysis as expected. For the low temperature data, the reflectance is much smaller (0.0007) near its minimum suggesting a k value of approximately 0.052 and shows that $n = 1$ occurs at a wavelength where $k < 0.1$. Of course, one should not infer that at $n = 1$ at R_{min} but only that $n - 1$ and k are small.

The results of the KK analysis of the three slags SA00, SA01, and SA05 are shown in Figures 9 and 10. From Figure 9 we see that the strong absorption band centered around 9-10 μm is broadened when compared to the low temperature data for the same slags. This band is primarily due to vibrational absorption by SiO_2. The absorption index, k, in this

wavelength range is not significantly different for the two slags SA00 and SA01, as expected. In the wavelength range below 10 μm the higher iron slag, SA05, has a smaller *k* than the two lower iron slags. This trend is in general agreement with the low temperature results of Goodwin. However, at wavelengths longer than 11 μm SA05 has a higher *k* than either SA00 or SA01. This trend is opposite for the low temperature data, where SA05 has a smaller *k* than SA00 or SA01. Generally, near 12 μm, the high temperature slag has *k* increasing with increasing iron content while the low temperature slag has *k* decreasing with increasing iron.

Figure 10 shows the computed *n* of the three synthetic slags. In the wavelength range below 6 μm there is little difference between the high and low temperature results. The refractive index, *n*, is approximately 1.5 near 1 μm and decreases with increasing wavelength until it reaches a minimum near 8.6 μm. However, there is a significant shift of the wavelength at which *n* passes through unity, with the higher temperature slags showing a marked shift to longer wavelengths. The weaker variation of *n* in the restrahlen absorption region is consistent with the broadened absorption band shown in Figure 9.

Another notable feature in Figure 10 is the variation of *n* with composition from 10-11.5 μm. In this wavelength range, *n* of SA05 is smaller than *n* of SA00 or SA01. This trend is not seen at all in the lower temperature data. We cannot currently explain this effect but will attempt to do so in a future QPR.

Summary

During the past quarter we have successfully measured the near normal reflectance of synthetic slags SA00, SA01, and SA05 at 1600°C. The expected similarity of the measurements for slags SA00 and SA01 (which have nearly the same composition) reinforces our conclusion that the experiment is repeatable, although more data will certainly be taken to ensure this. The Kramers-Kronig relations have been applied to the reflectance data to obtain *n* in the wavelength range 1-13 μm and *k* in the wavelength range 8-13 μm. The results show the expected strong SiO_2 absorption band in *k* and the related dispersion in *n*.

Currently we are examining the results from Task 1 to establish the slag compositions that are most representative of the majority of ash particles so that appropriate measurements can be made. Compositions will be limited to those which bear significantly on the radiation heat transfer in coal combustors. Once these compositions are established, a limited number of new synthetic slags will be made and their optical properties will be measured.

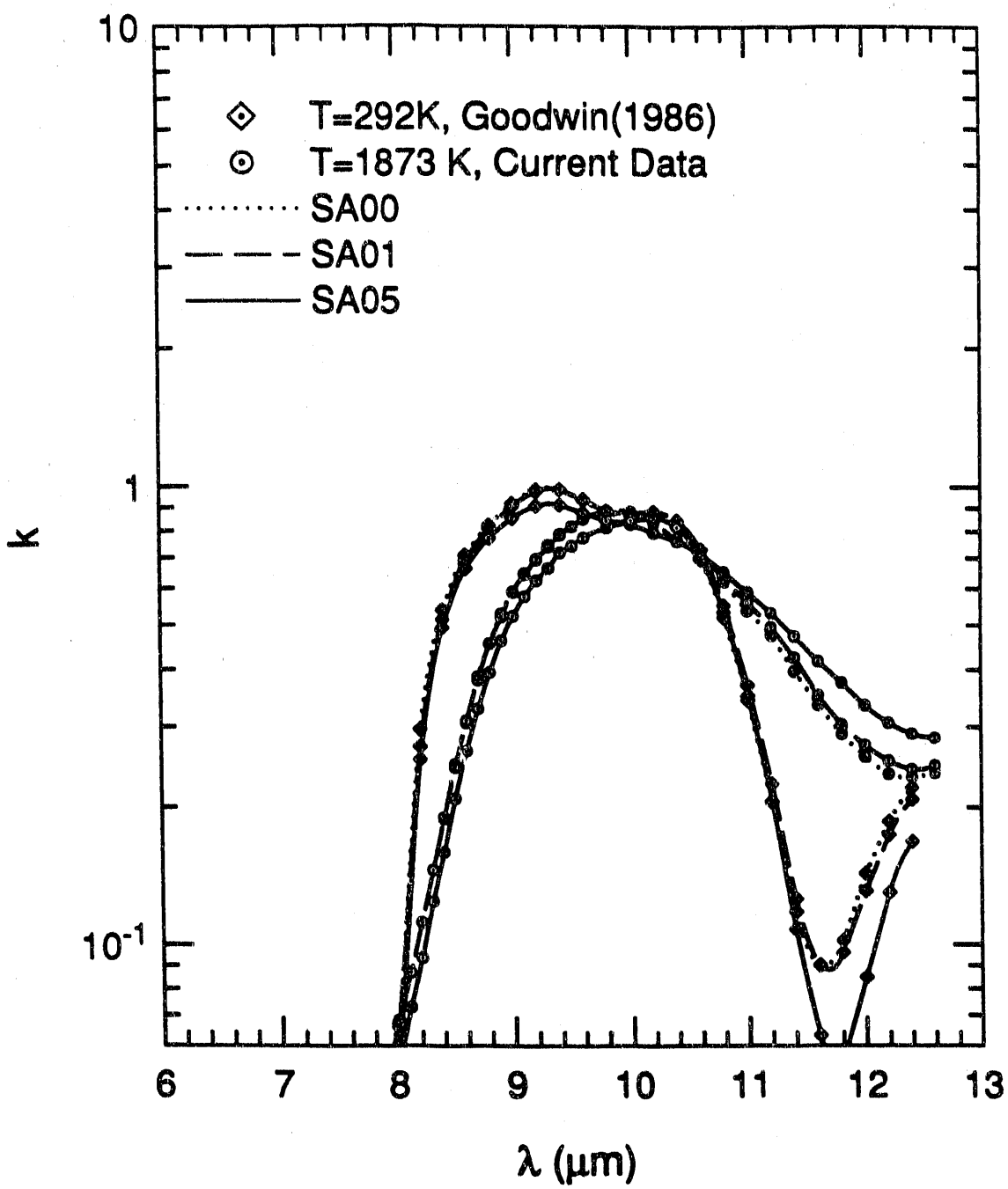

Figure 9. The absorption index, k, of molten synthetic slags SA00, SA01, and SA05 at 1600°C and of the same slags at room temperature.

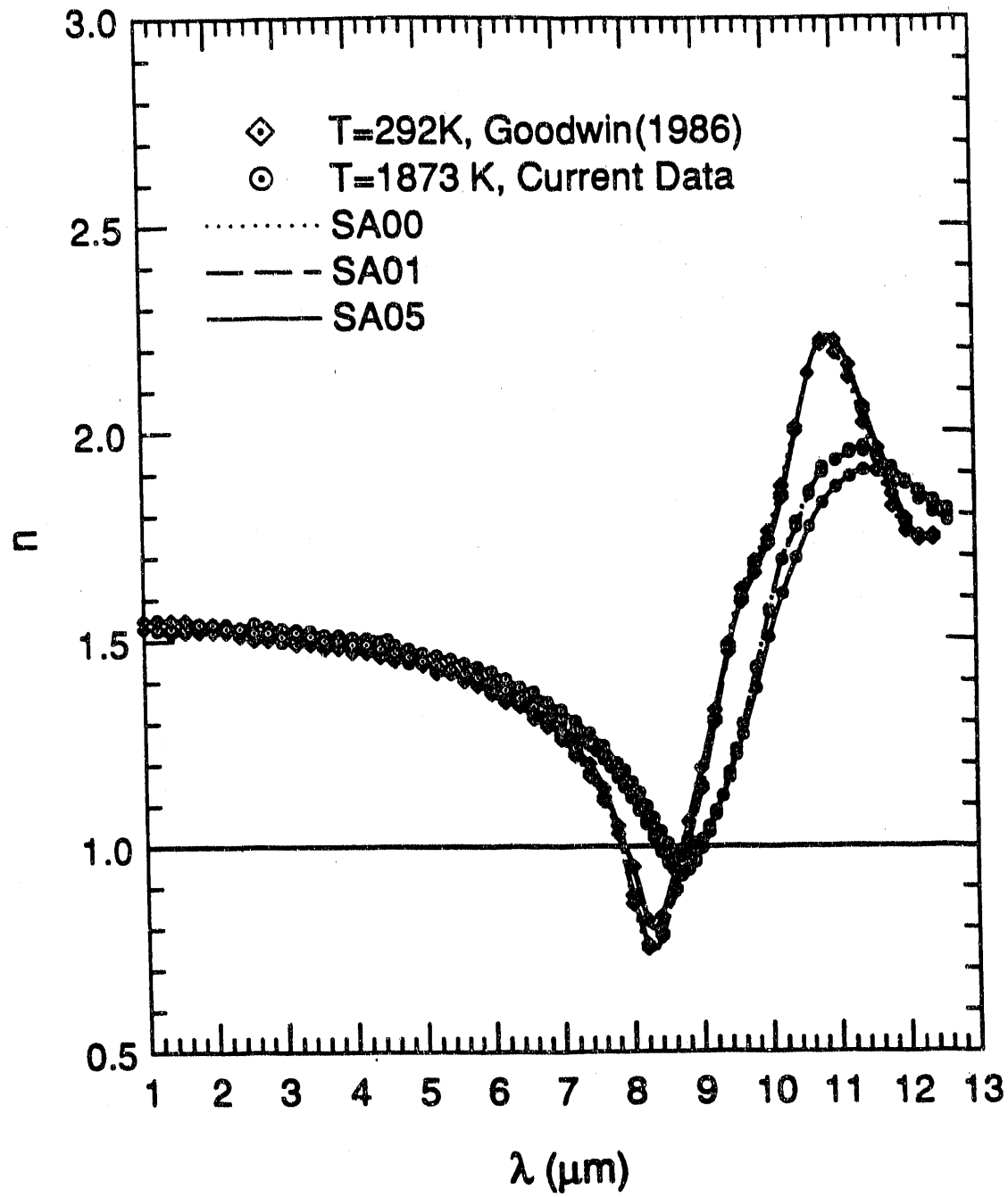

Figure 10. The real normal refractive index, *n*, of molten synthetic slags SA00, SA01, and SA05 at 1600°C and of the same slags at room temperature.

2.3 Task 3: Sample Calculations of the Radiant Properties of Flyash Dispersions

During the past year, several computer codes have been developed for this task. They were used to compute the effect on radiant transfer of varying the distribution of the iron content with particle size as reported in a paper presented at the Engineering Research Foundation Conference on "Mineral Matter and Ash in Coal" at Santa Barbara. These codes are also being used to determine the design conditions for Task 4.

2.4 Task 4: Measurement of the Radiant Properties of Flyash Dispersions

As noted earlier, the purpose of this task is to validate the whole approach adopted in this program. Specifically, this bench-scale experiment is intended to compare the measured optical/radiative properties of a dispersion of well characterized ash with those calculated on the basis of the known size/composition distribution using the correlation formulae relating the composition and complex refractive index resulting from measurements on bulk samples of synthetic slag (Task 2).

During the previous quarters, considerable thought has been given to the various possible approaches to satisfying the objectives of this task. Several experiments were done to guide our design of an apparatus for measuring the scattering and absorption properties of dispersions of flyash.

As a result of these experiments, and from extensive prior experience in connection with research on electrostatic precipitation, it has been determined that there is no satisfactory way to satisfy the aims of this task using a gaseous dispersion of flyash because it is not possible to adequately disperse and deagglomerate flyash into a gas stream. Unless the ash is adequately dispersed, as it exists in the radiant boiler of a pulverized coal-fired combustion system, one cannot expect calculations, based on Mie calculations for a dispersion of spheres to properly agree with laboratory measurements.

For these reasons, our design efforts for Task 4 are based on making measurements on a dispersion of flyash in liquid, for which our experience shows we can obtain stable, well-deagglomerated dispersions of ash. Because there is not single liquid which is adequately transparent over the wavelength range 1–12 μm, we plan to use a combination of three liquids, CCl_4, CS_2 and bromoform to cover the full range. Windows of BaF_2 will be used to contain the liquid suspension in an absorption/scattering cell.

A small flow loop, incorporating the measurement cell, an ultrasonic bath and a peristaltic pump is being assembled for this work which will employ the same infrared optical equipment used for measurements on slag samples under Task 2.

Infrared transmission measurements have been made on the three selected carrier liquids as reported in the last QPR.

In the past quarter, suitable infrared windows have been acquired and a preliminary design for an extinction cell has been evaluated. This cell is divided by a septum separating the flyash dispersion in one half from the pure liquid in the other half. The extinction due to the particles is then found by comparing the transmitted signals from the two halves of the cell when it is translated across the infrared beam.

END

DATE FILMED

12/23/92